Spin down of a stellar interior

Rosalind Oglethorpe

October 3, 2012

1 Introduction

Helioseismology has revealed a lot of information about the structure and dynamics of the solar interior, and we expect astroseismology from the Kepler probe to soon reveal similar information about other solar-type stars. The Sun and solar-type stars have two regions: a convective outer zone and a radiative inner zone [3, 10]. The radiative zone is stably stratified and energy transport is dominated by photon radiation.

Helioseismology has revealed that the convection zone is differentially rotating, as shown in Figure 1. At the equator, the rotation is fast with a period of about 25 days. The period increases with latitude, reaching about 30 days near the poles. The reason for this differential rotation is not yet completely understood. It is known that the turbulence in rotating convection is strongly anisotropic and causes a net flux of angular momentum towards the equator, but there are also many other processes involved in driving the differential rotation [8].

The radiative zone, by contrast, is in uniform rotation, as shown in Figure 1, with a period of about 27 days (the same as at approximately 30 degrees latitude in the convection zone). The two regions are separated by a rotational shear layer, which is called the tachocline [13]. Observations (for example, see Figure 1) reveal that the tachocline is very thin. This is surprising, because (as shown by [13]) the rotational shear should propagate into the interior on a relatively fast timescale, advected by meridional flows associated with the so-called 'thermal-spreading' process.

1.1 Thermal spreading

To understand thermal spreading, let's consider a thought-experiment in which, at time $t = 0$, the outer convection zone is differentially rotating and the inner radiative zone is uniformly rotating. Isobars in the uniformly rotating radiative zone are approximately spherical at first. As the differential rotation propagates into the top of the radiative zone, the Coriolis force due to the perturbation of the angular velocity must be compensated by a pressure perturbation, $\hat{P}$ (see Figure 2(a)). In hydrostatic equilibrium, the latter must be compensated by a change in the local density, and ultimately induces a temperature perturbation $\hat{T}$. The sign of the Coriolis force is such that the polar tachocline becomes somewhat hotter than the regions below, while the equatorial tachocline is somewhat cooler.

If the system is also in thermal equilibrium, advective and diffusive heat transport must compensate each other. As the temperature perturbation diffuses outwards, inward flows are

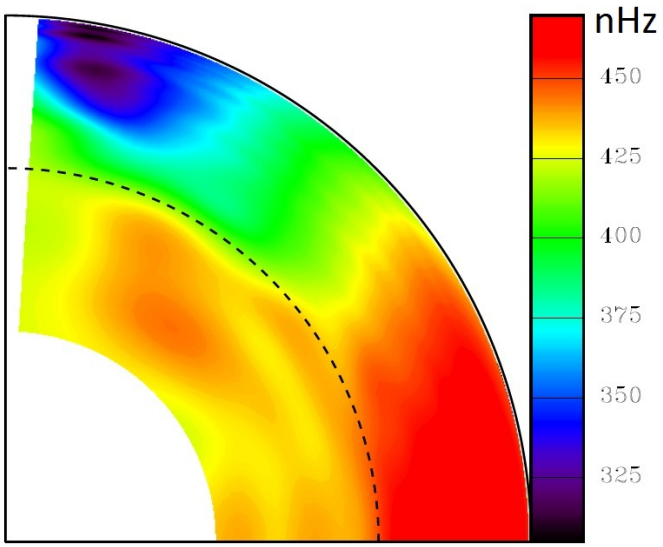

Figure 1: A graph of the angular velocity in the solar interior, from [3]. The outer convective zone is differentially rotating, and the inner radiative zone is uniformly rotating. The dashed line indicates the boundary between the convection zone and the radiative zone.

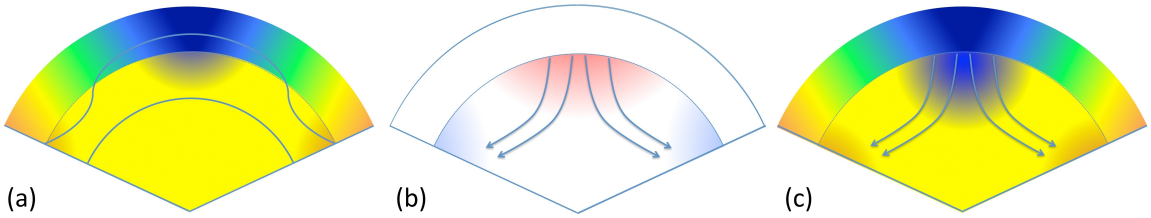

Figure 2: A schematic of the thermal spreading process. (a) Isobars are perturbed by the propagation of the differential rotation into the radiative zone (colour shows angular velocity and grey lines show isobars). (b) This pressure perturbation causes a temperature perturbation, and the diffusion of this temperature perturbation is balanced by inward flows to maintain thermal equilibrium (colour shows temperature perturbation and grey arrows show flows). (c) These inward flows advect the differential rotation further into the interior (third picture).

generated to balance the thermal diffusion (see Figure 2(b)). The latter transport angular momentum, so the differential rotation spreads into the radiative zone (see Figure 2(c)). Spiegel and Zahn [13] studied this process in detail. They found that the depth h of the tachocline grows via thermal spreading as

$$h \approx r_0 \left(\frac{t}{t_{ES}} \right)^{1/4}, \tag{1}$$

where r_0 is the radius of the radiative zone, t is time and

$$t_{ES} = \left(\frac{N}{2\Omega} \right)^2 \frac{r_0^2}{\kappa} \tag{2}$$

is the global Eddington-Sweet timescale. It is important to note here that viscosity plays no role in the process. By thermal spreading alone, Spiegel and Zahn argued that the thickness of the tachocline by now should be about a third of the total depth of the radiative zone. This is clearly at odds with observations from helioseismology (Figure 1). They concluded that there must be some other mechanism to stop the growth of the tachocline and the propagation of meridional flows into the interior.

1.2 The effect of an interior magnetic field: the Gough and McIntyre model

One mechanism that could impose a uniform rotation in the radiative zone is a primordial magnetic field, confined to the radiative zone [7]. The induction equation for a magnetic field is

$$\frac{\partial \mathbf{B}}{\partial t} = \nabla \times (\mathbf{u} \times \mathbf{B} - \eta \nabla \times \mathbf{B}), \tag{3}$$

where $\mathbf{u}$ is the velocity of the flow, $\mathbf{B}$ is the magnetic field and η is the magnetic diffusivity. For a steady axisymmetric magnetic field with negligible meridional flows and magnetic diffusivity, (3) simply becomes

$$\nabla \times (\mathbf{u} \times \mathbf{B}) = (\mathbf{B}.\nabla)\mathbf{u} - (\mathbf{u}.\nabla)\mathbf{B} = 0, \tag{4}$$

using the solenoidal condition $\nabla.\mathbf{B} = 0$. If we rewrite $\mathbf{u}$ as

$$\mathbf{u} = (0, 0, r \sin\theta \Omega), \tag{5}$$

in spherical coordinates (where Ω is the rotation rate), (4) yields Ferraro's law of isorotation [4],

$$\mathbf{B}.\nabla\Omega = 0, \tag{6}$$

which states that angular velocity is constant on magnetic field lines. Hence, as long as the magnetic field is confined to the radiative zone then (6) can enforce a uniform rotation in the interior. If the magnetic field lines are anchored in the convection zone, by contrast, (6) would promote the propagation of the differential rotation into the interior.

Unfortunately, by (3), magnetic fields diffuse over long timescales, so that any initially confined field slowly expands into the convection zone. Thus, differential rotation in the

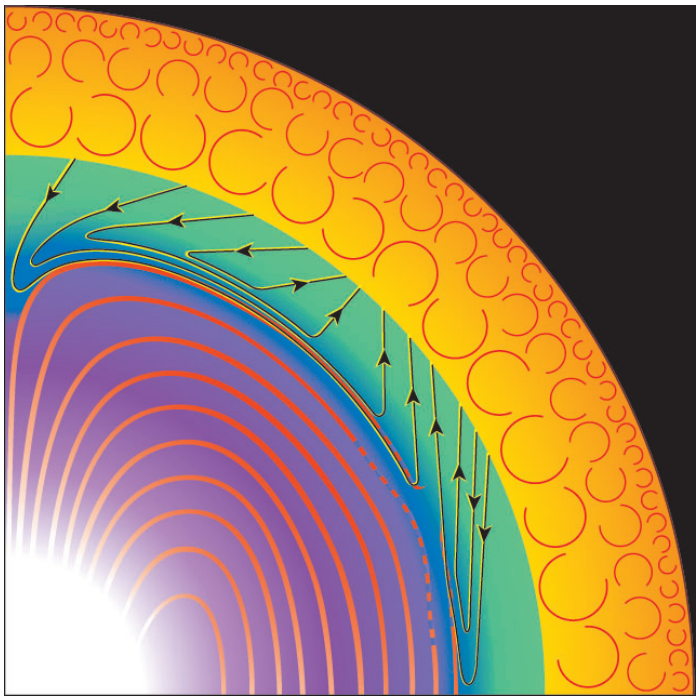

Figure 3: A schematic of the current tachocline paradigm, from [6]. The purple region is the magnetically dominated interior, with magnetic field lines shown in red. The blue region is the tachopause (thickness exaggerated by a factor of 50) and the green region is the tachocline (thickness exaggerated by a factor of 5). The arrows represent meridional flows in the tachocline. The yellow region is the convection zone.

radiative zone is expected unless there is a mechanism to keep the field actively confined against diffusion [2, 14]. Gough and McIntyre [6] showed that one way of keeping the field confined within the radiative zone is for the downwelling flows associated with the tachocline thermal spreading to balance the outward diffusion of the magnetic field.

A schematic of the current tachocline paradigm is shown in Figure 3, from [6]. In this model, the interior is magnetically dominated and in rigid rotation. Between this interior and the outer convection zone, there is a magnetic-free, stably stratified tachocline with thermally driven downwelling flows which confine the magnetic field. A thin magnetic boundary layer, called the tachopause, separates the tachocline from the rest of the interior.

1.3 The effect of spin down

The Gough and McIntyre model assumes that the system is in a steady state. However, there are several different possible sources of time-dependence in the problem, including the very slow (and complicated) timescale of the stellar evolution, the time for the diffusion of the magnetic field, the timescale of the decrease in rotation rate, and many others. We will focus on the effect of the decreasing rotation rate.

In addition to the internal primordial field, solar-type stars also host a distinct 'dynamo field' generated in the convection zone by turbulent fluid motions. In the Gough and McIn-

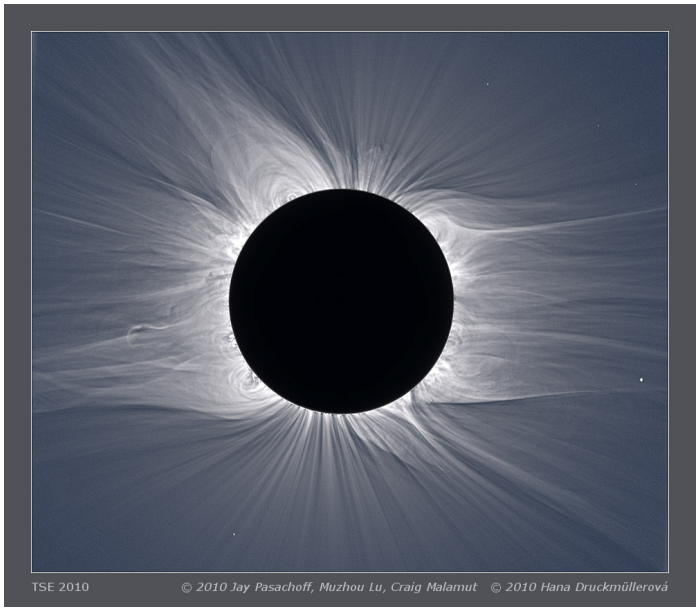

Figure 4: A photograph of the solar wind during the 11 July 2010 Solar eclipse, from [9].

tyre model, this magnetic field is assumed to be spatially separated from the primordial field by the magnetic-free tachocline. This dynamo field emerges at the surface and eventually becomes part of the solar wind. Figure 4 shows a photo of the solar wind during a solar eclipse. Charged particles travel along the field lines out from the star, and their angular velocity slows down by conservation of angular momentum. However, by Ferraro's law of isorotation, the angular velocity must be constant along field lines. This exerts a magnetic torque on the outer layers of the star, causing them to slow down.

Skumanich [11] looked at the rotation rates of several clusters of solar-type stars, and found that the mean stellar rotation rate decays as a power law with time, as

$$\Omega \sim t^{-1/2}. \tag{7}$$

This project aims to look at the effect of spin down on the model by [6]. In what follows, we first study how spin down propagates into a non-magnetic interior, and then look at what happens if a magnetic field is included in the radiative zone.

2 Stratified, non-magnetic spin down

We first consider the spin down of a stratified, non-magnetic star. We build upon the work of Bretherton and Spiegel [1], which is now discussed for clarity and completeness.

2.1 Spin-down of an unstratified, non-magnetic star

Bretherton and Spiegel [1] were the first to study the spin down of an unstratified star. They consider a star with an outer convection zone and an inner radiative zone, and model it as an unstratified sphere of fluid (which represents the radiative zone) surrounded by a

spherical shell of porous medium (the convection zone). The interior region has radius a, and the total radius of the star is b. Since $Pr \ll 1$, the viscosity is negligible.

The porous medium is rotating with an angular velocity $\Omega(t)$, which slows down over time as

$$\Omega(t) = \Omega_0 \exp(-kt), \tag{8}$$

where Ω_0 is the initial rotation rate and k is the spin down rate. The spin down is assumed to be slow, so that $k \ll \Omega_0$. Bretherton and Spiegel look for a 'steady state', where the $D\mathbf{u}/Dt$ term is negligible in the momentum equation expressed in a frame rotating with angular velocity $\Omega(t)$. The 'steady state' equations of motion in the porous medium are Darcy's law and the incompressibility condition:

$$\frac{1}{\tau}\mathbf{u} = -\frac{1}{\rho}\nabla\hat{P}, \quad \nabla.\mathbf{u} = 0, \tag{9}$$

where τ is the Darcy friction timescale and $\hat{P}$ is the pressure perturbation away from hydrostatic equilibrium. The equations of motion in the interior are

$$2\mathbf{\Omega} \times \mathbf{u} - k\mathbf{\Omega} \times \mathbf{r} = -\frac{1}{\rho}\nabla\hat{P}, \quad \nabla.\mathbf{u} = 0. \tag{10}$$

The first term in (10) is the Coriolis force, and the second is Euler's force which is due to the deceleration of the frame. Solving these equations, then matching $\hat{P}$ and the normal velocity at the interface between the interior and the porous medium, $r = a$, yields for instance the angular velocity perturbation $\hat{\Omega}(r, \theta, t)$ everywhere in the star. The angular velocity in the interior turns out to be uniform, with value

$$\hat{\Omega}_c = \frac{3a^5 + 2b^5}{b^5 - a^5}\frac{k}{4\Omega\tau}, \tag{11}$$

in the rotating frame. Since $\hat{\Omega}_c > 0$, there is a constant lag in the propagation of the spin down into the interior.

In short, the porous medium and the interior are each uniformly rotating, but the interior is always rotating faster, since $\hat{\Omega}_c$ is always positive. The lag depends on the rate of spin down, k, the rotation rate of the porous medium, Ω, and the Darcy relaxation time scale of the porous medium, τ.

2.2 Spin down of a stratified non-magnetic star (cylindrical model)

2.2.1 The model

We now consider a similar model to [1], but with a stratified interior and with differential rotation in the convection zone. Because of the added complexity, we have to model a cylinder instead of a full sphere, with gravity parallel to the rotation axis. This adds a geometrical error, but on the other hand allows for a fully analytical solution. This cylinder can be viewed as the polar regions of the star. The lower part is filled with stratified fluid, with constant buoyancy frequency N and negligible viscosity ν, from $z = 0$ to $z = z_{cz}$, and with a porous medium from $z = z_{cz}$ to $z = 1$. Figure 5 is a diagram of the model set up.

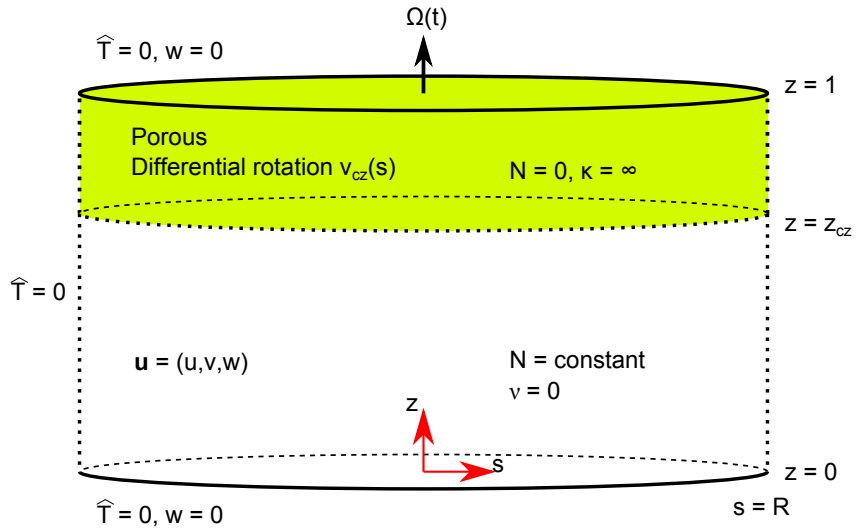

Figure 5: A diagram of the cylindrical model set up. The region from $z = 0$ to $z = z_{cz}$ is filled with a stably stratified fluid, with constant buoyancy frequency N, and the viscosity ν is negligible. The region from $z = z_{cz}$ to $z = 1$ (yellow) is filled with a differentially rotating porous medium.

The porous medium is rotating with angular velocity $\Omega(t)$, and following [1] we work in a frame rotating with angular velocity $\Omega(t)$. The cylinder has radius R and unit height. We use cylindrical coordinates (s, ϕ, z) in the rotating frame, and assume axisymmetry with respect to the axis of rotation (which is in the vertical z direction) so that $\partial/\partial\phi = 0$. In these coordinates, we write the velocity relative to the rotating frame as $\mathbf{u} = (u, v, w)$.

The real dynamics of a stellar convection zone are very complicated. Our main goal here is to model rapid momentum transport from the surface down to the top of the radiative zone. The simplest possible model that has such a property is one with a Darcy friction term, as in [1, 5]. We replace the effect of the Reynolds stresses with a Darcy forcing term in the convection zone ($z > z_{cz}$), so that in this region the velocity of the fluid relaxes to the assumed velocity of the porous medium on a timescale τ. In the rotating frame, we consider that the porous medium may be also differentially rotating, with velocity $v_{cz}(s)\hat{\mathbf{e}}_\phi$. We require the net angular momentum of the porous medium in the rotating frame to be zero, so the differential rotation does not apply any torque to the system. The porous medium represents the convection zone, where $N \approx 0$, and (for simplicity) we also take its thermal diffusivity to be effectively infinite[1], so that the temperature perturbation $\hat{T} = 0$ for $z > z_{cz}$. The momentum equation for the fluid in the porous medium is then

$$\frac{\partial \mathbf{u}}{\partial t} + 2\mathbf{\Omega} \times \mathbf{u} + \dot{\mathbf{\Omega}} \times \mathbf{r} + \frac{\mathbf{u} - v_{cz}(s)\mathbf{e}_\phi}{\tau} = -\frac{1}{\rho}\nabla \hat{P}. \tag{12}$$

In the 'bulk' of the fluid ($z < z_{cz}$) we make several assumptions to simplify the equations (as in, for example, [1], [6] and [13]). We use the Boussinesq approximation (for

[1]This assumption gives the solution to lowest order in κ_b/κ_p, where κ_p and κ_b are the thermal diffusivities in the porous medium and the plug, respectively, and $\kappa_p \gg \kappa_b$

example, [12]) and assume that the fluid is incompressible everywhere. We assume that the Rossby number, which is the ratio of the Coriolis acceleration to the advective term, is small. Under this assumption, flows are sufficiently slow that we can neglect the non-linear advective term in the momentum equation. We assume the flow is hydrostatic and geostrophic, so viscous forces are much less important than Coriolis forces. We also assume that the flows are sufficiently steady and slow for the system to be in thermal equilibrium, with heat diffusion being balanced by the advection of the background entropy.

The momentum equation in the bulk is then

$$\frac{\partial \mathbf{u}}{\partial t} + 2\mathbf{\Omega} \times \mathbf{u} + \dot{\mathbf{\Omega}} \times \mathbf{r} = -\frac{1}{\rho}\nabla \hat{P} + \frac{g}{T}\hat{T}\hat{\mathbf{e}}_z, \tag{13}$$

where T is the mean temperature and ρ is the mean density.

We choose the boundary conditions to have zero temperature perturbation, $\hat{T}$, and vertical velocity, w, at $z = 0$ and $z = 1$. We solve the equations separately for $z > z_{cz}$ and $z < z_{cz}$, and match $\hat{T}$, w and pressure perturbation $\hat{P}$ at the radiative-convective interface z_{cz}. In short,

$$\hat{T} = 0 \text{ at } z = 0, z = 1, \tag{14}$$

$$w = 0 \text{ at } z = 0, z = 1, \tag{15}$$

$$\hat{T}(z = z_{cz}^-) = \hat{T}(z = z_{cz}^+), \tag{16}$$

$$\hat{P}(z = z_{cz}^-) = \hat{P}(z = z_{cz}^+), \tag{17}$$

$$w(z = z_{cz}^-) = w(z = z_{cz}^+). \tag{18}$$

Boundary conditions at the side wall $s = R$ are more difficult to choose, as we want them to have as little influence as possible on the flow inside the cylinder. We choose

$$\hat{T} = 0 \text{ at } s = R. \tag{19}$$

This boundary condition allows a radial flow across the side wall, which by conservation of mass must be zero overall. We assume that the flow into and out of the cylinder through the side walls has negligible influence on the flow in the cylinder. From (13) the radial and vertical momentum equations in the bulk are

$$\frac{1}{\rho}\frac{\partial \hat{P}}{\partial z} = \frac{g}{T}\hat{T}, \tag{20}$$

$$2\Omega v = \frac{1}{\rho}\frac{\partial \hat{P}}{\partial s}. \tag{21}$$

Using the side wall boundary condition (19) in (20) gives $\hat{P} = 0$ at $s = R$. Combining (20) and (21) yields the thermal wind equation

$$2\Omega\frac{\partial v}{\partial z} = \frac{g}{T}\frac{\partial \hat{T}}{\partial s}. \tag{22}$$

We also have the equations for thermal equilibrium,

$$\frac{N^2 T}{g} w = \kappa \nabla^2 \hat{T}, \tag{23}$$

where κ is the thermal diffusivity in the bulk, and incompressibility

$$\frac{1}{s}\frac{\partial}{\partial s}(su) + \frac{\partial w}{\partial z} = 0. \tag{24}$$

Combining (22), (23) and (24) gives an equation relating u and v

$$-N^2\frac{\partial}{\partial s}\left(\frac{1}{s}\frac{\partial}{\partial s}(su)\right) = 2\Omega\kappa\left(\frac{\partial^4 v}{\partial z^4} + \frac{\partial}{\partial z}\frac{\partial}{\partial s}\left(\frac{1}{s}\frac{\partial}{\partial s}(sv)\right)\right). \tag{25}$$

The first term on the right hand side is equivalent to the thermal spreading term found in [13], and indicates that there is transport of angular momentum by downwelling meridional flows. A second equation for u and v comes from the ϕ-component of the angular momentum equation (13),

$$\frac{\partial v}{\partial t} + 2\Omega u + \dot{\Omega} s = 0. \tag{26}$$

We then combine (25) and (26) to find v.

2.2.2 'Steady state' solution

Following [1] we first look for a 'steady state' solution, where (26) becomes

$$2\Omega u + \dot{\Omega} s = 0. \tag{27}$$

This immediately gives

$$u = -\frac{s}{2}\frac{\dot{\Omega}}{\Omega}, \tag{28}$$

and conservation of mass, with the boundary condition (15), gives

$$w = \frac{\dot{\Omega}}{\Omega} z. \tag{29}$$

Note that the frame is slowing down, so $\dot{\Omega} < 0$. Solving (23) with boundary conditions (19) then gives

$$\hat{T} = \sum_n J_0\left(\lambda_n \frac{s}{R}\right)\left[\alpha_n \sinh \lambda_n \frac{z}{R} - \frac{C_n z R^2}{\lambda_n^2}\right], \tag{30}$$

with λ_n the zeros of the Bessel function $J_0(x)$ and

$$C_n = \frac{N^2 T}{g\kappa}\frac{\dot{\Omega}}{\Omega}\frac{2}{\lambda_n J_1(\lambda_n)}. \tag{31}$$

The unknown coefficients α_n can be related to C_n using the boundary condition (16). Since $\hat{T} = 0$ in the porous medium:

$$\alpha_n = \frac{C_n z_{cz} R^2}{\lambda_n^2}\frac{1}{\sinh \lambda_n \frac{z_{cz}}{R}}. \tag{32}$$

Equations (20) and (21) then give $\hat{P}$ and v, up to the unknown set of integration constant $\{p_n\}$:

$$\frac{1}{\rho}\hat{P} = \frac{g}{T}\sum_n J_0(\lambda_n \frac{s}{R}) \left[\frac{\alpha_n R}{\lambda_n}\cosh\lambda_n \frac{z}{R} - \frac{C_n z^2 R^2}{2\lambda_n^2} + p_n\right], \tag{33}$$

$$v = \frac{g}{2\Omega T}\sum_n \frac{dJ_0(\lambda_n \frac{s}{R})}{ds} \left[\frac{\alpha_n R}{\lambda_n}\cosh\lambda_n \frac{z}{R} - \frac{C_n z^2 R^2}{2\lambda_n^2} + p_n\right]. \tag{34}$$

To find v, by finding p_n, we also need to solve the equations in the porous medium.

In the porous medium, $\hat{T} = 0$, and the ϕ-component of the momentum equation (12) in steady state reduces to

$$2\Omega u + \dot{\Omega} s = -\frac{v - v_{cz}(s)}{\tau}, \tag{35}$$

where τ is the time scale of the Darcy force. For ease of algebra, we assume that τ is sufficiently small that, to the lowest order[2] in τ, and

$$v \cong v_{cz}(s). \tag{36}$$

From (12), the radial and vertical momentum equations are

$$\frac{1}{\rho}\frac{\partial \hat{P}}{\partial z} = -\frac{w}{\tau}, \tag{37}$$

$$\frac{1}{\rho}\frac{\partial \hat{P}}{\partial s} = -\frac{u}{\tau} + 2\Omega v_{cz}(s). \tag{38}$$

Combining these with incompressibility $\nabla.\mathbf{u} = 0$ gives

$$\nabla^2 w = 0. \tag{39}$$

Using the boundary condition (15), we can write w as

$$w = \sum_n B_n \sinh\left[\lambda_n\left(\frac{z}{R} - \frac{1}{R}\right)\right] J_0\left(\lambda_n \frac{s}{R}\right), \tag{40}$$

for some constants B_n and λ_n. Equation (37) then gives

$$\frac{1}{\rho}\hat{P} = \sum_n J_0\left(\lambda_n \frac{s}{R}\right)\left[-\frac{B_n}{\tau}\frac{R}{\lambda_n}\cosh\left[\lambda_n\left(\frac{z}{R} - \frac{1}{R}\right)\right] + P_n\right], \tag{41}$$

and using the boundary condition (17) at $s = R$ gives that λ_n are the zeros of $J_0(x)$ as in the bulk solution. Incompressibility also gives

$$u = \sum_n \frac{dJ_0(\lambda_n \frac{s}{R})}{ds}\frac{R}{\lambda_n} B_n \cosh\left[\lambda_n\left(\frac{z}{R} - \frac{1}{R}\right)\right], \tag{42}$$

[2]This expansion is not necessary, and the calculation can be done without it. However, the solutions are not as simple and lose clarity.

so that (38) becomes

$$\frac{1}{\rho}\frac{\partial \hat{P}}{\partial s} + \frac{u}{\tau} = \sum_n \frac{dJ_0(\lambda_n \frac{s}{R})}{ds} P_n = 2\Omega(t) v_{cz}(s), \tag{43}$$

which uniquely defines P_n,

$$P_n = -\frac{4\Omega(t)}{\lambda_n J_1^2(\lambda_n)} \int_0^R \frac{s}{R} v_{cz}(s) \lambda_n J_1\left(\lambda_n \frac{s}{R}\right) ds. \tag{44}$$

Matching w and $\hat{P}$ at $z = z_{cz}$ gives

$$B_n = \frac{\dot{\Omega}}{\Omega} \frac{2 z_{cz}}{\lambda_n J_1(\lambda_n) \sinh \lambda_n \left(\frac{z_{cz}}{R} - \frac{1}{R}\right)}, \tag{45}$$

and

$$p_n = \frac{T}{g} P_n - \frac{T}{g} \frac{B_n R}{\tau \lambda_n} \cosh\left[\lambda_n \left(\frac{z_{cz}}{R} - \frac{1}{R}\right)\right] - \frac{\alpha_n R}{\lambda_n} \cosh\left(\lambda_n \frac{z_{cz}}{R}\right) + \frac{C_n z^2 R^2}{2\lambda_n^2}, \tag{46}$$

so that the azimuthal velocity (34) becomes

$$\begin{aligned} v = &- \frac{1}{\Omega} \sum_n \frac{J_1(\lambda_n \frac{s}{R})}{\lambda_n J_1(\lambda_n)} \frac{\dot{\Omega}}{\Omega} \left[\frac{N^2}{\kappa} \frac{z_{cz} R^2}{\lambda_n^2} \left(\frac{\cosh \lambda_n \frac{z}{R} - \cosh \lambda_n \frac{z_{cz}}{R}}{\sinh \lambda_n \frac{z_{cz}}{R}} - \frac{\lambda_n}{2 z_{cz} R} (z^2 - z_{cz}^2) \right) \right. \\ &\left. - \frac{1}{\tau} \frac{z_{cz}}{\tanh \lambda_n (\frac{z_{cz}}{R} - \frac{1}{R})} \right] + v_{cz}(s). \end{aligned} \tag{47}$$

2.2.3 Physical interpretation of the 'steady-state' solution

In order to understand this solution more physically, let's define the different time scales in this problem as

$$t_{sd} = -\frac{\Omega}{\dot{\Omega}},\ t_{ES} = \left(\frac{N}{2\Omega}\right)^2 \frac{R^2}{\kappa},\ t_\Omega = \frac{1}{\Omega},\ t_\tau = \tau, \tag{48}$$

where t_{sd} is the spin down timescale, t_{ES} is the global Eddington-Sweet timescale, which is the timescale for thermal spreading [13], t_Ω is the rotation timescale and t_τ is the Darcy friction timescale. We re-write (47) in terms of these timescales,

$$\begin{aligned} v = &\frac{1}{t_{sd}} \sum_n \frac{J_1(\lambda_n \frac{s}{R})}{\lambda_n J_1(\lambda_n)} \left[\frac{t_{ES}}{t_\Omega} \frac{4 z_{cz}}{\lambda_n^2} \left(\frac{\cosh \lambda_n \frac{z}{R} - \cosh \lambda_n \frac{z_{cz}}{R}}{\sinh \lambda_n \frac{z_{cz}}{R}} - \frac{\lambda_n}{2 z_{cz} R} \left(z^2 - z_{cz}^2\right) \right) \right. \\ &\left. - \frac{t_\Omega}{t_\tau} \frac{z_{cz}}{\tanh \lambda_n (\frac{z_{cz}}{R} - \frac{1}{R})} \right] + v_{cz}(s). \end{aligned} \tag{49}$$

This expression shows that v has two separate parts, one which depends on the spin down and one which depends on the differential rotation. We first consider the case with no differential rotation, $v_{cz}(s) = 0$, to isolate the effect of the spin down. Equation (49) shows that v depends on t_{sd} as well as ratios of the other three timescales, t_{ES}/t_Ω and t_Ω/t_τ.

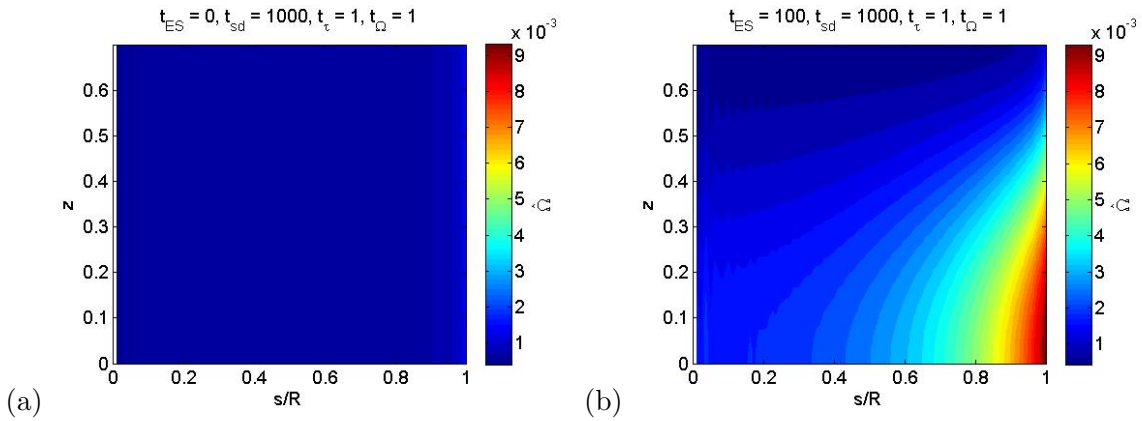

Figure 6: Contour plots of $\hat{\Omega}$ in the 'steady state' solution. (a) Unstratified case. $\hat{\Omega}$ is constant with depth and strictly positive everywhere. (b) Stratified case. $\hat{\Omega}$ is strictly positive everywhere, and increases with depth and cylindrical radius.

If there is no stratification in the bulk, $t_{ES} = 0$ and $v(s, z = 0) = v(s, z = z_{cz}) = v(s) > 0$. This implies that the azimuthal velocity is independent of depth, as expected from the Taylor-Proudman constraint, and that there is a lag in the interior with respect to the porous medium. The angular velocity perturbation, $\hat{\Omega} = v/s$, is

$$\hat{\Omega} = \frac{t_\Omega}{t_\tau t_{sd}} \sum_n \frac{J_1(\lambda_n \frac{s}{R})}{s\lambda_n J_1(\lambda_n)} \frac{z_{cz}}{\tanh \lambda_n (\frac{1}{R} - \frac{z_{cz}}{R})}, \tag{50}$$

which is similar to the result from [1]. Indeed, $\hat{\Omega}$ contains the same ratio of timescales as in [1] but with a different geometrical factor, which is naturally expected since we are using a cylinder rather than a sphere.

If the bulk is stratified, $t_{ES} > 0$, then $v(s, z = 0) > v(s, z = z_{cz}) > 0$, showing that the lag increases with depth. This can be interpreted in two ways. On the one hand, one may view that the spin down is propagated more quickly to the top of the bulk, near the porous medium, than to the bottom which is further away. Alternatively one may also consider that as the stratification increases, the thermal wind (22) can support more vertical shear, so the lag at the bottom increases. Figure 6 shows contour plots of $\hat{\Omega}$ in the bulk for $t_{ES} = 0$ and $t_{ES} > 0$. For $t_{ES} = 0$, Figure 6(a) shows an approximately uniform lag, which is constant with depth. For $t_{ES} > 0$, Figure 6(b) shows that the lag increases with both depth and with s.

2.2.4 Time-dependent solution

Having found the 'steady state' solution, we now return to the time-dependent equations to find when this 'steady state' is valid. We expand v again on the same basis of Bessel functions, as

$$v = \sum_n \frac{dJ_0(\lambda_n \frac{s}{R})}{ds} \tilde{v}_n(z, t). \tag{51}$$

Combining (25) and (26) with this ansatz gives

$$\frac{\partial \tilde{v}_n}{\partial t} + \left(\frac{2\Omega(t)R}{N\lambda_n}\right)^2 \kappa \frac{\partial^4 \tilde{v}_n}{\partial z^4} - \left(\frac{2\Omega(t)}{N}\right)^2 \kappa \frac{\partial^2 \tilde{v}_n}{\partial z^2} = \frac{\dot{\Omega} R^2}{\lambda_n^2} \frac{4}{\lambda_n J_1(\lambda_n)}. \tag{52}$$

The first and second terms on the left hand side recover the equation found by [13] for the thermal spreading of differential rotation into the interior using a boundary layer approximation, and the third term on the right hand side completes the full expression for thermal spreading in the absence of a boundary layer approximation. The right hand side contains the global forcing term arising from Euler's force. Thus the evolution of the angular momentum in the bulk has two contributions: a transport by meridional flows, which is the thermal spreading found by [13], and a global extraction of angular momentum by the spinning down of the frame.

To solve (52), we need to express all boundary conditions in terms of $v_n(z)$. The boundary conditions at $z = 0$ are

$$\hat{T} = 0 \Rightarrow \frac{\partial \tilde{v}_n}{\partial z} = 0, \tag{53}$$

$$w = 0 \Rightarrow \frac{\partial^3 \tilde{v}_n}{\partial z^3} = 0. \tag{54}$$

In the porous medium, by contrast, we assume that the dynamics always relax to the steady state on a very rapid timescale. Hence (40), (41) and (42) hold. The boundary conditions at $z = z_{cz}$ are then

$$\hat{T} \text{ continuous} \Rightarrow \hat{T} = 0 \Rightarrow \frac{\partial \tilde{v}_n}{\partial z} = 0, \tag{55}$$

$$\hat{P} \text{ continuous} \Rightarrow \frac{\partial \hat{P}}{\partial s} \text{ continuous} \Rightarrow 2\Omega \tilde{v}_n = -\frac{B_n R}{\tau \lambda_n} \cosh\left[\lambda_n \left(\frac{z_{cz}}{R} - \frac{1}{R}\right)\right] + P_n, \tag{56}$$

$$w \text{ continuous} \Rightarrow \frac{2\Omega\kappa}{N^2} \frac{\partial^3 \tilde{v}_n}{\partial z^3} = B_n \sinh\left[\lambda_n \left(\frac{z_{cz}}{R} - \frac{1}{R}\right)\right], \tag{57}$$

using (55). Equations (56) and (57) combine to give

$$\tilde{v}_n + \frac{R}{\tau \lambda_n} \frac{1}{\tanh[\lambda_n(\frac{z_{cz}}{R} - \frac{1}{R})]} \frac{\kappa}{N^2} \frac{\partial^3 \tilde{v}_n}{\partial z^3} = \frac{P_n}{2\Omega(t)}, \tag{58}$$

where the right hand side is independent of time if $v_{cz}(s)$ is independent of time in the spinning down frame, from (41). The true steady state solution with these inhomogeneous boundary conditions is

$$v = v_{cz}(s), \tag{59}$$

so that, if the differential rotation remains constant while the rotation rate of the frame decays, eventually the forcing from the spin down is negligible compared to the forcing from the differential rotation, and the angular velocity in the bulk is the same as in the porous medium. We write

$$v = \sum_n \frac{dJ_0(\lambda_n \frac{s}{R})}{ds} \tilde{v}_n(z,t) = \sum_n \frac{dJ_0(\lambda_n \frac{s}{R})}{ds} \hat{v}_n(z,t) + v_{cz}(s), \tag{60}$$

where $\hat{v}_n$ obeys (52) with homogeneous boundary conditions

$$\frac{\partial \hat{v}_n}{\partial z} = 0 \qquad \text{at } z = 0,\ z = z_{cz}, \tag{61}$$

$$\frac{\partial^3 \hat{v}_n}{\partial z^3} = 0 \qquad \text{at } z = 0, \tag{62}$$

$$\frac{\partial^3 \hat{v}_n}{\partial z^3} = -\frac{N^2}{\kappa}\frac{\tau \lambda_n}{R}\tanh\left[\lambda_n\left(\frac{z_{cz}}{R} - \frac{1}{R}\right)\right]\hat{v}_n \qquad \text{at } z = z_{cz}, \tag{63}$$

from (53), (54), (55) and (58).

Equation (52) is separable, so we can write

$$\hat{v}_n = \sum_m T_{nm}(t) Z_{nm}(z), \tag{64}$$

where the eigenfunctions $Z_{nm}(z)$ satisfy

$$\frac{\partial^2}{\partial z^2}\left(\left(\frac{\lambda_n}{R}\right)^2 - \frac{\partial^2}{\partial z^2}\right) Z_{nm}(z) = -\left(\frac{\mu_{nm}}{R^2}\right)^2 Z_{nm}(z) \tag{65}$$

for some constants μ_{nm}. The operator on the left hand side is self-adjoint with the boundary conditions (61) - (63). As with the horizontal modes, we can project onto the vertical modes to find an evolution equation for $T_{nm}(t)$. Since (65) is an equation with constant coefficients, we seek solutions of the form

$$Z_{nm}(z) = \mathrm{e}^{\sigma_{nm} z}, \tag{66}$$

and find four solutions for σ_{nm}: $\pm\sigma_{1,nm}$ and $\pm i\sigma_{2,nm}$, where

$$\sigma_{1,nm} = \frac{1}{R}\left[\frac{\lambda_n^2}{2} + \sqrt{\mu_{nm}^2 + \frac{\lambda_n^4}{4}}\right]^{1/2},\ \sigma_{2,nm} = \frac{1}{R}\left[\sqrt{\mu_{nm}^2 + \frac{\lambda_n^4}{4}} - \frac{\lambda_n^2}{2}\right]^{1/2}, \tag{67}$$

and where μ_{nm} can be determined using (63). Applying the boundary conditions (61) - (63) we finally find

$$Z_{nm}(z) = \left[\frac{\sigma_{2,nm}}{\sigma_{1,nm}}\frac{\sin \sigma_{2,nm} z_{cz}}{\sinh \sigma_{1,nm} z_{cz}}\cosh \sigma_{1,nm} z + \cos \sigma_{2,nm} z\right]. \tag{68}$$

Projecting (52) onto these eigenfunctions $Z_{nm}(z)$ gives

$$\dot{T}_{nm}(t) + \left(\frac{2\Omega(t)\mu_{nm}}{NR\lambda_n}\right)^2 \kappa T_{nm}(t) = \frac{\dot{\Omega} R^2}{\lambda_n^2}\frac{4}{\lambda_n J_n(\lambda_n)}\frac{\int_0^{z_{cz}} Z_{nm}(z)dz}{\int_0^{z_{cz}} Z_{nm}^2(z)dz} \equiv G_{nm}(t), \tag{69}$$

where $G_{nm}(t)$ is the projection of the global forcing term in (52) onto the vertical modes. Equation (69) can be solved using an integrating factor method to give

$$T_{nm}(t) = \exp\left(-\left(\frac{2\mu_{nm}}{NR\lambda_n}\right)^2 \kappa \int^t \Omega^2(t')dt'\right) \times \tag{70}$$

$$\left[\int_{t_0}^t G_{nm}(t') \exp\left(\left(\frac{2\mu_{nm}}{NR\lambda_n}\right)^2 \kappa \int^{t'} \Omega^2(t'')dt''\right) dt' + T_{0,nm}\right], \tag{71}$$

with

$$T_{0,nm} = \exp\left(\left(\frac{2\mu_{nm}}{NR\lambda_n}\right)^2 \kappa \int^{t_0} \Omega^2(t)dt\right) \frac{\int_0^{z_{cz}} v(t=t_0)Z_n(z)dz}{\int_0^{z_{cz}} Z_n^2(z)dz}. \tag{72}$$

2.2.5 Physical interpretation of the solutions

As discussed in section 1, there is strong observational and theoretical evidence suggesting that $\Omega(t)$ decays as a power law, with $\Omega(t) = \Omega_0(t/t_0)^{-\alpha}$ for some $\alpha > 0$. In this case,

$$\int^t \Omega^2(t')dt' = \begin{cases} \frac{\Omega^2(t)t}{1-2\alpha} & (\alpha \neq \frac{1}{2}), \\ \Omega^2(t)t\log(t) & (\alpha = \frac{1}{2}), \end{cases} \tag{73}$$

so we expect fundamentally different behaviour for $\alpha \neq 1/2$ and $\alpha = 1/2$. As in (48), the spin down timescale and the global Eddington-Sweet timescale are

$$t_{sd}(t) = -\frac{\Omega(t)}{\dot{\Omega}(t)} = \frac{t}{\alpha},\ t_{ES}(t) = \left(\frac{NR}{2\Omega(t)}\right)^2 \frac{1}{\kappa} = \left(\frac{NR}{2\Omega_0}\right)^2 \frac{t^{2\alpha}}{\kappa t_0^{2\alpha}}, \tag{74}$$

where each of them now explicitly depends on time. We also define the local Eddington-Sweet time of each mode as

$$t_{ES}^{nm}(t) = \left(\frac{NR}{2\Omega(t)}\right)^2 \frac{\lambda_n^2}{\mu_{nm}^2\kappa}. \tag{75}$$

Writing $T_{nm}(t)$ in terms of these timescales yields,

$$T_{nm}(t) = \begin{cases} \exp\left(-\frac{\alpha}{1-2\alpha}\frac{t_{sd}}{t_{ES}^{nm}}\right)\left[G_{nm}(t)t^{\alpha+1}\int_{t_0}^t t'^{-\alpha-1}\exp\left(\frac{\alpha}{1-2\alpha}\left(\frac{t_{sd}}{t_{ES}^{nm}}\right)'\right) + T_{0,nm}\right] & (\alpha \neq \frac{1}{2}), \\ t^{-t_{sd}/2t_{ES}^{nm}}\left[G_{nm}(t)t^{3/2}\int_{t_0}^t t'^{\left(t_{sd}/2t_{ES}^{nm}\right)'-3/2} + T_{0,nm}\right] & (\alpha = \frac{1}{2}). \end{cases} \tag{76}$$

We see that the behaviour of each mode $T_{nm}(t)$ depends on both α and the ratio of timescales

$$\frac{t_{sd}(t)}{t_{ES}^{nm}(t)} = \frac{1}{\alpha}\left(\frac{2\Omega_0}{NR}\right)^2 \frac{\mu_{nm}^2\kappa}{\lambda_n^2} t_0^{2\alpha} t^{1-2\alpha}, \tag{77}$$

which itself changes over time for $\alpha \neq 1/2$.

If $\alpha > 1/2$, which corresponds to rapid spin down, (76) shows that the effect of the initial conditions exponentially increases on a timescale of t_{sd}/t_{ES}^{nm}. Although the latter decreases over time, it remains strictly positive so the solution always blows up. This suggests that our original assumptions, for example that $\mathbf{u}.\nabla\mathbf{u}$ is negligible, must break down in the case of rapid spin down, and our solution is not valid. If $\alpha < 1/2$, which corresponds to slow spin down, the initial conditions always decay exponentially and the system relaxes to a 'steady' state, where only the global forcing term and the differential rotation influence the system.

Finally, if $\alpha = 1/2$, as suggested by Skumanich's law [11], we can write

$$T_{nm}(t) = \frac{g_{nm}\Omega(t)}{t_{sd}/2t_{ES}^{nm} - 1/2} + t^{-t_{sd}/2t_{ES}^{nm}}\left[T_{0,nm} - \frac{g_{nm}\Omega_0}{t_{sd}/2t_{ES}^{nm} - 1/2} t_0^{t_{sd}/2t_{ES}^{nm}}\right], \tag{78}$$

with g_{nm} defined as

$$g_{nm} \equiv \frac{G_{nm}(t)t}{\Omega(t)}, \tag{79}$$

which is independent of time. In this case, t_{sd}/t_{ES}^{nm} is also independent of time as seen from (77), so the initial ratio of these two timescales determines the behaviour. The initial conditions decay on a timescale of $t_{sd}/2t_{ES}^{nm}$ for each mode. Since

$$t_{ES}^{nm} < t_{ES} \, \forall n, m, \tag{80}$$

then if

$$\frac{t_{sd}}{t_{ES}} \gg 1, \tag{81}$$

we also have

$$\frac{t_{sd}}{t_{ES}^{nm}} \gg 1 \, \forall \, \mu_{nm}, \lambda_n. \tag{82}$$

In other words, if $t_{sd} \gg t_{ES}$ then the time dependent solution decays to our previous 'steady state' solution, which is equivalent to

$$T_{nm}(t) = \frac{g_{nm}\Omega(t)}{t_{sd}/2t_{ES}^{nm}}. \tag{83}$$

If, on the other hand, $t_{sd}/t_{ES} \ll 1$ then there are two classes of modes: small-scale modes for which $t_{sd}/t_{ES}^{nm} > 1$ and large-scale modes for which $t_{sd}/t_{ES}^{nm} < 1$. When $t_{sd}/t_{ES}^{nm} > 1$, (78) shows that the initial conditions decay faster than the global forcing term, so that after some time these small-scale modes are governed only by the global forcing and the differential rotation. However, when $t_{sd}/t_{ES}^{nm} < 1$, the global forcing term in (78) decays faster than the initial conditions, so the initial conditions continue to influence the system even after a long time and the 'steady state' solution found in 2.2.2 is not as relevant.

Up to this point in our model, the radiative interior has played no role in the angular momentum transport, and shear propagates to the centre of the star. However, in the magnetized model of a stellar interior by [6] (see Figure 3), the shear only propagates through the tachocline as far as the tachopause, and there interacts with the magnetic field which keeps the interior in solid body rotation. We now want to incorporate the angular momentum transport between the tachocline and the interior into our model, to find out how spin down affects the rotation of the interior below the tachocline. We return to our cylindrical model of a stellar interior, where the porous medium at the top of the cylinder still corresponds to the convection zone, where the 'bulk of the fluid' corresponds to the stably stratified, non-magnetic tachocline only, and where we now add an additional 'ingredient' to model the interior.

3 Unstratified Ekman layer spin down

In the model by [6], angular momentum transport between the tachocline and the interior is caused by magnetic stresses within a thin boundary layer (the tachopause). There, the primordial magnetic field interacts with the flows in the tachocline, and helps transmit the spin-down information from the outer layers downward. Since magnetic torques are

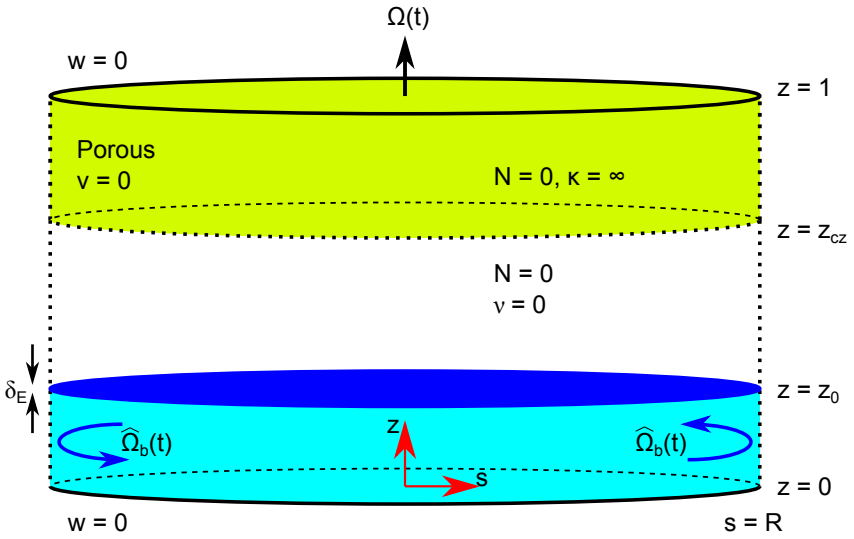

Figure 7: A diagram of the adjusted cylindrical model set up. The region from $z = 0$ to $z = z_0$ (light blue) is a solid base which is free to rotate at angular velocity $\hat{\Omega}_b(t)$ in the rotating frame. The region from $z = z_0$ to $z = z_{cz}$ is filled with unstratified fluid, and the viscosity ν is negligible except for near the base. There is a thin boundary layer above the base, with thickness δ_E, where the viscous forces become dominant. The region from $z = z_{cz}$ to $z = 1$ (yellow) is filled with a porous medium which has zero angular velocity in the rotating frame.

intrinsically nonlinear, to aid our conceptual understanding, we first consider the case of viscous torques.

Our model set up is very similar to the model investigated in the previous section. The bottom of the cylinder now hosts a solid inner cylinder of radius R and thickness z_0, see Figure 7, shaped like a hockey-puck. The density of the 'hockey-puck' is same as the density of the fluid, and it is free to rotate at an angular velocity $\hat{\Omega}_b(t)$ in the rotating frame. Our goal is to find $\hat{\Omega}_b(t)$.

We consider as a first simplified system the unstratified case, where the bulk (from $z = z_0$ to $z = z_{cz}$) is filled with unstratified fluid. For simplicity we assume that there is no differential rotation of the porous medium, although the differential rotation can be included without altering the steps of the calculation significantly. The torque between the fluid and the hockey-puck is communicated through a thin (Ekman) boundary layer of thickness δ_E at $z = z_0$. In this layer viscosity becomes important, and we can no longer neglect the viscous terms in the momentum equation.

In the bulk ($z_0 < z < z_{cz}$), we look for a 'steady state' solution as in section 2.2.2, which is now known to be a valid approximate solution as long as the spin down rate is slow enough. For $z > z_0 + \delta_E$, the equations of motion are the same as in section 2.2.2, setting $\hat{T} = 0$ since the bulk is unstratified. Equation (20) becomes

$$\frac{\partial \hat{P}}{\partial z} = 0 \Rightarrow \hat{P} = \hat{P}_0(s) \Rightarrow v = v_0(s), \tag{84}$$

and, as in the previous 'steady state' solution,

$$u = -\frac{\dot{\Omega}}{2\Omega}s \Rightarrow w = w_0(s) + \frac{\dot{\Omega}}{\Omega}(z - (z_0 + \delta_E)), \tag{85}$$

where $w_0(s)$ is the vertical velocity at the top of the viscous boundary layer (at $z = z_0 + \delta_E$).

To find an evolution equation for $\hat{\Omega}_b(t)$, we begin by writing the complete angular momentum conservation equation as

$$\frac{\partial}{\partial t}(sv + s^2\Omega) + \nabla.(\mathbf{u}\Omega s^2 + \text{viscous terms}) = 0. \tag{86}$$

Assuming that the tachocline (i.e. the bulk) is in 'steady' state while retaining the time dependence of the interior implies that the thermal spreading across the bulk is faster than angular momentum transport across the interior, which we will check a posteriori.

We then integrate (86) over the volume of the hockey-puck and the boundary layer. The viscous terms are negligible at the top of the boundary layer, and we assume that they are also negligible at the side wall in the boundary layer:

$$\int_0^{2\pi}\int_0^{z_0+\delta_E}\int_0^{R} \frac{\partial}{\partial t}(sv + s^2\Omega) + \nabla.(\mathbf{u}\Omega s^2 + \text{viscous terms})dV = 0, \tag{87}$$

$$\Rightarrow z_0\frac{R^4}{4}\left(\frac{d\hat{\Omega}_b}{dt} + \dot{\Omega}\right) + \int_0^R w_0(s)\Omega s^3 ds + R\int_{z_0}^{z_0+\delta_E} u(s=R)\Omega R^2 dz = 0, \tag{88}$$

using the fact that $\delta_E \ll z_0$ (see section 3.1).

There is no flow into the hockey-puck, so the amount of fluid going into the boundary layer through the surface $z = z_0 + \delta_E$ must be the same as the amount of fluid coming out through the side, by conservation of mass

$$2\pi\int_0^R w_0(s)sds = -2\pi R\int_{z_0}^{z_0+\delta_E} u(s=R)dz. \tag{89}$$

Combining this with (88) gives

$$\frac{d\hat{\Omega}_b}{dt} = -\dot{\Omega} + \frac{4\Omega}{R^4 z_0}\left(R^2\int_0^R w_0(s)sds - \int_0^R w_0(s)s^3 ds\right). \tag{90}$$

In order to proceed, we need to determine $w_0(s)$. In order to do this, we now investigate the dynamics of the boundary layer in more detail.

3.1 Boundary layer thickness

In the boundary layer, the viscous term cannot be neglected and becomes an integral part of the momentum balance. Assuming that the boundary layer is thin, so that $\partial/\partial z \gg \partial/\partial s$, and assuming a 'steady state', we have

$$2\mathbf{\Omega}\times\mathbf{u} + \dot{\mathbf{\Omega}}\times\mathbf{r} = -\frac{1}{\rho}\nabla\hat{P} + \nu\frac{\partial^2\mathbf{u}}{\partial z^2}. \tag{91}$$

The three components of the momentum equation (91) are

$$-2\Omega v = -\frac{1}{\rho}\frac{\partial \hat{P}}{\partial s} + \nu\frac{\partial^2 u}{\partial z^2}, \tag{92}$$

$$2\Omega u + \dot{\Omega} s = \nu\frac{\partial^2 v}{\partial z^2}, \tag{93}$$

$$0 = -\frac{1}{\rho}\frac{\partial \hat{P}}{\partial z} + \nu\frac{\partial^2 w}{\partial z^2}. \tag{94}$$

Combining these three equations with conservation of mass gives

$$-\frac{\partial v}{\partial z} = \frac{\nu^2}{4\Omega^2}\frac{\partial^5 v}{\partial z^5}. \tag{95}$$

Let $\delta_E = \sqrt{\nu/2\Omega}$ and $Z = (z - z_0)/\delta_E = O(1)$ in the boundary layer. Then

$$\frac{\partial v}{\partial Z} + \frac{\partial^5 v}{\partial Z^5} = 0 \tag{96}$$

$$\Rightarrow v = v_0(s) + \sum_{n=0}^{3} b_n(s)\mathrm{e}^{\lambda_n Z}, \quad \lambda_n = \mathrm{e}^{(2n+1)i\pi/4}. \tag{97}$$

$v \to v_0(s)$ as $Z \to \infty$, where $v_0(s)$ is the azimuthal velocity in the bulk, so $b_3 = b_4 = 0$, and $v \in \mathbb{R}$, so $b_1 = b_2$. Finally, at $Z = 0$, which is the top of the hockey-puck, $v = s\hat{\Omega}_b(t)$. Using all this information uniquely specifies the boundary layer solution to be:

$$v(s, Z) = v_0(s) + (\hat{\Omega}_b s - v_0(s))\mathrm{e}^{-Z/\sqrt{2}}\cos\left(\frac{Z}{\sqrt{2}}\right). \tag{98}$$

3.2 Jump condition

The hockey-puck rotates with angular velocity $\hat{\Omega}_b(t)$ in the rotating frame, which is as yet unknown. Integrating the angular momentum equation (93) across the viscous boundary layer gives

$$\int_{z_0}^{z_0+\delta_E} su\,dz + \frac{\dot{\Omega}}{2\Omega}s^2\delta_E = \frac{\nu}{2\Omega}\left[\frac{\partial v}{\partial z}\right]_{z_0}^{z_0+\delta_E} = \frac{\nu}{2\Omega}\frac{1}{\delta_E}\left[\frac{\partial v}{\partial Z}\right]_{Z=0}^{Z\to\infty} = \frac{\delta_E}{\sqrt{2}}(\Omega_b s - v_0(s)). \tag{99}$$

Using conservation of mass and the boundary condition $w = 0$ at $z = z_0$, we find

$$\frac{1}{s}\frac{\partial}{\partial s}\int_{z_0}^{z_0+\delta_E} su\,dz = -\int_{z_0}^{z_0+\delta_E}\frac{\partial w}{\partial z}dz = -w(z_0 + \delta_E) \equiv -w_0(s), \tag{100}$$

so that, combining (99) and (100),

$$w_0(s) = \frac{\dot{\Omega}}{\Omega}\delta_E - \frac{\delta_E}{\sqrt{2}}\frac{1}{s}\frac{\partial}{\partial s}(\Omega_b s^2 - s v_0(s)). \tag{101}$$

We now know the vertical velocity profile $w_0(s)$ in terms of the differential rotation $v_0(s)$ in the bulk of the fluid. The latter still remains to be determined, by matching the bulk solution to the porous medium.

The solutions in the porous medium are found exactly as in section 2, and we consider the case where $v_{cz}(s) = 0$,

$$w = \sum_n J_0\left(\lambda_n \frac{s}{R}\right) B_n \sinh\left[\lambda_n\left(\frac{z}{R} - \frac{1}{R}\right)\right], \tag{102}$$

$$u = \sum_n \frac{dJ_0(\lambda_n \frac{s}{R})}{ds} \frac{B_n R}{\lambda_n} \cosh\left[\lambda_n\left(\frac{z}{R} - \frac{1}{R}\right)\right], \tag{103}$$

$$\frac{1}{\rho}\hat{P} = \sum_n J_0\left(\lambda_n \frac{s}{R}\right)\left[-\frac{B_n R}{\tau\lambda_n}\cosh\left[\lambda_n\left(\frac{z}{R} - \frac{1}{R}\right)\right]\right]. \tag{104}$$

We can then match w and $\hat{P}$ at $z = z_{cz}$ to find the solutions for $w_0(s)$, $\hat{P}_0(s)$ and $v_0(s)$ in the bulk:

$$\frac{1}{\rho}\hat{P}_0(s) = \sum_n J_0\left(\lambda_n \frac{s}{R}\right)\left[-\frac{B_n R}{\tau\lambda_n}\cosh\left[\lambda_n\left(\frac{z_{cz}}{R} - \frac{1}{R}\right)\right]\right] \tag{105}$$

$$\Rightarrow v_0(s) = \frac{1}{2\Omega}\sum_n \frac{dJ_0(\lambda_n \frac{s}{R})}{ds}\left[-\frac{B_n R}{\tau\lambda_n}\cosh\left[\lambda_n\left(\frac{z_{cz}}{R} - \frac{1}{R}\right)\right]\right], \tag{106}$$

$$\sum_n J_0\left(\lambda_n \frac{s}{R}\right) B_n \sinh\left[\lambda_n\left(\frac{z_{cz}}{R} - \frac{1}{R}\right)\right] = w_0(s) + \frac{\dot{\Omega}}{\Omega}(z_{cz} - (z_0 + \delta_E)), \tag{107}$$

from (85). Combining these equations with the jump condition (101) gives an equation for $v_0(s)$,

$$v_0(s) = \sum_n \frac{2J_1(\lambda_n \frac{s}{R})}{\lambda_n J_1(\lambda_n)}\left[\frac{2\delta_E\hat{\Omega}_b - \sqrt{2}\frac{\dot{\Omega}}{\Omega}(z_{cz} - z_0)}{2\sqrt{2}\Omega\tau\tanh\lambda_n(\frac{1}{R} - \frac{z_{cz}}{R}) + \frac{\delta_E}{R}\lambda_n}\right], \tag{108}$$

which is similar to (47) in section 2, with no stratification ($N = 0$), but now with two extra terms which depend on δ_E and $\hat{\Omega}_b$. Using (108) in (101) to find $w_0(s)$, (90) finally yields the desired evolution equation for $\hat{\Omega}_b(t)$:

$$\frac{d\hat{\Omega}_b}{dt} = -\dot{\Omega}\frac{z_{cz}}{z_0} - 32\sum_n \frac{1}{\lambda_n^4}\left[\frac{-\dot{\Omega}\left(\frac{z_{cz}}{z_0} - 1\right) + \sqrt{2}\delta_E\frac{\hat{\Omega}_b\Omega}{z_0}}{1 + \frac{\delta_E\lambda_n}{2\sqrt{2}R\Omega\tau\tanh\lambda_n(\frac{1}{R} - \frac{z_{cz}}{R})}}\right], \tag{109}$$

Note that if there is no viscous boundary layer, so $\delta_E = 0$, it can be shown using the identity $32\sum_n 1/\lambda_n^4 = 1$ that $d\hat{\Omega}_b/dt = -\dot{\Omega}$. In other words, the hockey-puck continues to rotate at its initial angular velocity as the frame slows down, since the fluid cannot exert any torque on it. However, if $\delta_E > 0$ then the evolution of $\hat{\Omega}_b$ is affected by the boundary layer. Figure 8 shows a plot of $\hat{\Omega}_b/\Omega$ with time for arbitrary parameters, starting with initial condition $\hat{\Omega}_b(t_0) = 0$ and assuming that the frame is spinning down as $\Omega(t) = \Omega_0\sqrt{t_0/t}$. The 'steady' solution, where $d\hat{\Omega}_b/dt$ is neglected, is also plotted. We see that $\hat{\Omega}_b$ relaxes to the 'steady' solution on the Ekman timescale across the thickness of the hockey-puck,

$$t_\nu = \frac{z_0}{\sqrt{\nu\Omega}}. \tag{110}$$

This is consistent with assuming a 'steady' state for both the hockey-puck and the bulk, so in fact we did not need to consider the time-dependence of the interior in (86)-(88). The

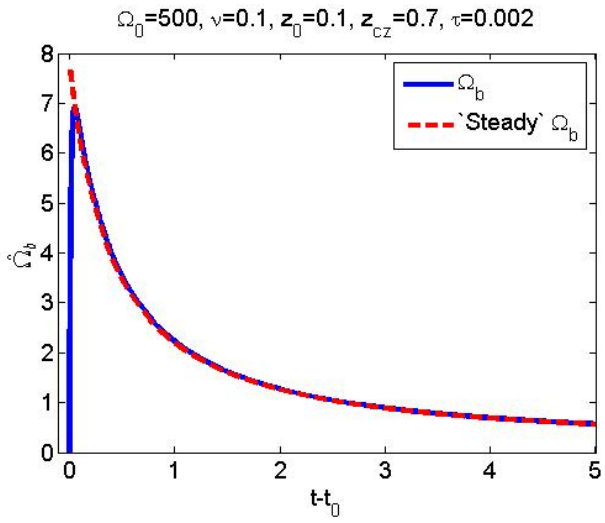

Figure 8: A plot of $\hat{\Omega}_b$ with time (blue solid line) and the corresponding 'steady' solution (red dashed line), for arbitrary parameters, with initial condition $\hat{\Omega}_b(t_0) = 0$ and with a spin-down rate of the frame $\Omega(t) = \Omega_0\sqrt{t_0/t}$. $\hat{\Omega}_b$ relaxes to the 'steady' state on the Ekman timescale.

'steady' solution decays with time so that the rotation rate of the base (relative to that of the frame) decreases with time as $\Omega(t)$ decreases. In other words, the lag between the two, given by $\hat{\Omega}_b$, also decreases over time.

4 Unstratified magnetic spin down

4.1 Solution in the tachocline and tachopause

In a solar-type star, we expect that the torque acting on the interior is due to magnetic stresses rather than viscous friction. We now consider a similar set up to that of section 3 where the hockey-puck is replaced by a fluid held in rigid rotation by a confined large-scale magnetic field, in the region from $z = 0$ to $z = z_0$, and where the Ekman boundary layer is replaced by a magnetic 'tachopause' at $z = z_0$. Assuming that the magnetic field does not exert a torque at the side wall of the cylinder in the boundary layer and that the thickness of the magnetic boundary layer δ is small compared with $z_{cz} - z_0$ or z_0, the evolution equation for $\hat{\Omega}_b$ is the same as with the viscous boundary layer (90). The difference between the magnetic and the viscous cases comes from the angular momentum transport across the boundary layer, which we now discuss.

Wood *et al.* [15] studied a system very similar to the Gough and McIntyre model [6], but in Cartesian coordinates. They found that the thickness of the magnetic boundary layer is given by

$$\delta = \sqrt{\frac{2\pi\rho\eta\Omega R^2}{B_0^2}}, \tag{111}$$

assuming a horizontal magnetic field with strength B_0 at the bottom of the magnetic bound-

ary layer. They also found a jump condition relating the vertical and 'azimuthal' velocities in the tachocline. This jump condition takes exactly the same form as the Ekman jump condition in Cartesian coordinates, namely:

$$w_0(x) = \frac{1}{\sqrt{2}}\delta_E \frac{\partial v_0(x)}{\partial x} \text{ (Ekman)} \quad \text{and} \quad w_0(x) = \frac{\pi}{4}\delta \frac{\partial v_0(x)}{\partial x} \text{ (magnetic)}, \tag{112}$$

where x is the latitudinal direction and v_0 is the azimuthal velocity, and where $\dot{\Omega} = \hat{\Omega}_b = 0$ in the Wood *et al.* model. Hence, by analogy with the way the Cartesian Ekman jump condition can be transformed into cylindrical coordinates, it can be shown that, in cylindrical coordinates, the tachopause jump conditions including the effect of spin-down are:

$$w_0(s) = \frac{\dot{\Omega}}{\Omega}\delta + \frac{\pi}{4}\delta \frac{1}{s}\frac{\partial}{\partial s}\left(s v_0(s) - \hat{\Omega}_b s^2\right). \tag{113}$$

From section 3, we have the solutions in the bulk and in the porous medium, and using this jump condition, we now find

$$v_0(s) = \sum_n \frac{2J_1(\lambda_n \frac{s}{R})}{\lambda_n J_1(\lambda_n)} \left[\frac{2\pi\delta\hat{\Omega}_b - 4\frac{\dot{\Omega}}{\Omega}(z_{cz} - z_0)}{8\Omega\tau \tanh\lambda_n(\frac{1}{R} - \frac{z_{cz}}{R}) + \pi\frac{\delta}{R}\lambda_n}\right], \tag{114}$$

which, as in the case with a viscous boundary layer, is similar to (47) with $N = 0$, but now with two extra terms which depend on δ and $\hat{\Omega}_b$. Equation (90) becomes

$$\frac{d\hat{\Omega}_b}{dt} = -\dot{\Omega}\frac{z_{cz}}{z_0} - 32\sum_n \frac{1}{\lambda_n^4}\left[\frac{-\dot{\Omega}\left(\frac{z_{cz}}{z_0} - 1\right) + \frac{\pi}{2}\delta\frac{\hat{\Omega}_b\Omega}{z_0}}{1 + \frac{\pi\delta\lambda_n}{8R\Omega\tau\tanh\lambda_n(\frac{1}{R} - \frac{z_{cz}}{R})}}\right]. \tag{115}$$

This evolution equation for $\hat{\Omega}_b$ depends on δ, z_0 and B_0. If we assume that z_0 and B_0 are known, we get δ from (111) and can then evolve $\hat{\Omega}_b(t)$ as in section 3.

4.2 Where is the tachopause?

Unfortunately, by contrast with section 3, z_0 is not actually known a priori - it results from the nonlinear interaction of the field and the downwelling flows. However, while the full solution needs fully nonlinear calculations, we can make an order of magnitude estimate using the magnetic induction equation as in [6] and [15].

The steady magnetic induction equation is, from (3),

$$0 = \nabla \times (\mathbf{u} \times \mathbf{B} - \eta\nabla \times \mathbf{B}), \tag{116}$$

where $\mathbf{B}$ is the magnetic field and η is the magnetic diffusivity. We need the vertical velocity at the top of the magnetic boundary layer to balance the magnetic field diffusion for the magnetic field to remain confined. This implies $w \approx \eta/\delta$. We cannot choose $w_0(s) = \eta/\delta \,\forall\, s$, as the s-dependence of $w_0(s)$ is determined by the solutions above the boundary layer. Instead, we set the average of w to be η/δ, so that

$$\int_0^R s w_0(s) ds = \frac{R^2}{2}\frac{\eta}{\delta}. \tag{117}$$

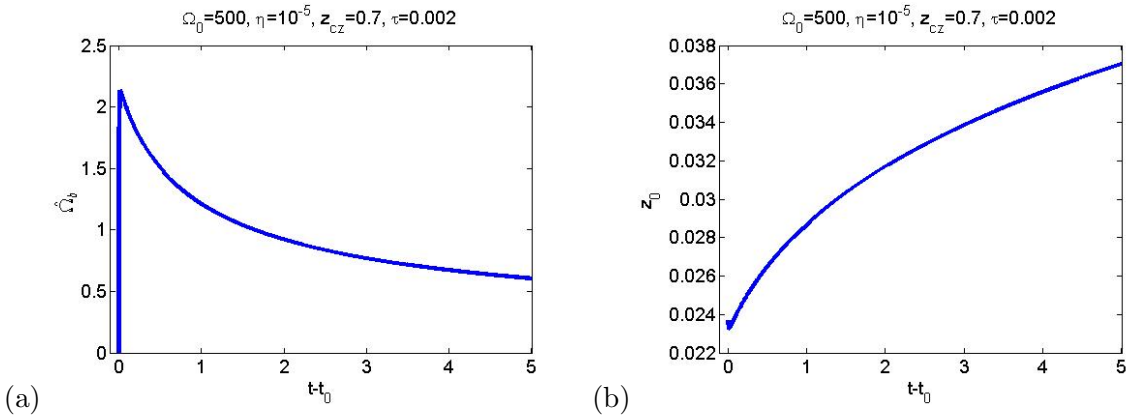

(a) (b)

Figure 9: (a) A plot of $\hat{\Omega}_b$ with time and (b) a plot of z_0 with time, with $\rho = 1$ and $B_0^2 = 100\pi$.

Equation (113) becomes

$$\frac{\eta}{\delta} = -\frac{\dot{\Omega}}{\Omega}(z_{cz} - (z_0 + \delta)) + \sum_n \frac{32}{\lambda_n^2}\left[\frac{\dot{\Omega}(z_{cz} - z_0) - \frac{\pi}{2}\delta\hat{\Omega}_b\Omega}{8\Omega + \frac{\pi\delta\lambda_n}{R\tau\tanh\lambda_n(\frac{1}{R} - \frac{z_{cz}}{R})}}\right]. \tag{118}$$

Equations (115) and (118) are two equations for the two unknowns, $\hat{\Omega}_b$ and z_0, so the system is now fully determined in terms of the internal field strength B_0. Figure 9(a) shows a plot of $\hat{\Omega}_b$ with time, assuming a constant B_0. As in Figure 8, $\hat{\Omega}_b$ initially increases rapidly from zero, as in section 3, then starts to decrease with time, so that the lag in the angular velocity between the magnetically dominated region ($z < z_0$) and the porous medium decreases over time. The corresponding depth of the magnetically dominated region, z_0 (shown in Figure 9(b)), increases with time as $\hat{\Omega}_b$ and Ω decrease. However, to find the long-time behaviour of $\hat{\Omega}_b$ and z_0, we would also need to consider how B_0 changes with time, as this will also affect how z_0 and δ, and therefore also $\hat{\Omega}_b$, change with time.

5 Summary and future work

We have proposed a solution for the spin down of a stratified star. Although we have modelled it as a cylinder with a porous medium at the top, we now discuss our results in the context of real stellar interiors. We first looked at non-magnetic stellar radiative zones. We found that there exists a 'steady state' solution. As in Bretherton and Spiegel, these solutions exhibit a lag in the angular velocity between the convection zone and radiative zone below, with the latter always rotating faster than the former. If stratification is very weak, this lag is uniform with depth and agrees with the result from the spherical model found by [1], up to a geometrical factor. When the radiative zone is strongly stratified, the lag increases with depth because the thermal wind can maintain a larger vertical shear.

We have also found time-dependent solutions. The evolution of the angular momentum in the radiative zone has contributions from both transport by meridional flows, through the thermal spreading found by [13] for the propagation of differential rotation into the interior

of a star, and global angular momentum extraction by the spin down of the frame. We have found that $\Omega(t) \sim t^{-1/2}$, which is the case for solar-type stars (see [11]), is a special case for the time-dependent solution. A more rapid spin-down rate cannot be accommodated by a laminar solution, while a slower spin-down rate implies that the system can rapidly converge to the 'steady state' solution described above. For $\Omega \sim t^{-1/2}$, the initial conditions decay with time as a power law, rather than the exponential decay found for $\Omega(t) \sim t^{-\alpha}$ with $\alpha < 1/2$.

We then studied the spin down of an unstratified magnetic star. We assume that the radiative interior is held in rigid rotation by a large-scale magnetic field, separated by a non-magnetic tachocline. We found that the spin-down of the frame is transmitted to the magnetically dominated region due to magnetic friction in a magnetic boundary layer separating the tachocline from the interior. The lag between the convection zone and the interior decreases with time, and our solutions are consistent with a 'steady' state in both the bulk of the fluid and the interior.

The next step is to combine the stratified and magnetic solutions to find a solution, in our cylindrical model, for the spin down of a stratified, magnetic star. In addition, we need to model the interior magnetic field in more detail and to look at how the magnetic field decays with time, and how this affects and is affected by the depths of the tachocline and magnetic boundary layer. It would also be interesting to solve an equivalent spherical model (as in [1] but with a stratified interior) numerically, which would represent the whole star, and compare this solution to our solution for a cylinder which represents the polar regions of the star.

6 Acknowledgements

I would like to thank Pascale Garaud for her supervision on this project, and all the staff and fellows for such an inspiring and enjoyable summer.

References

[1] F. P. Bretherton and E. A. Spiegel, *The effect of the convection zone on solar spin-down*, The Astrophysical Journal, 153 (1968), pp. 77–80.

[2] A. S. Brun and J.-P. Zahn, *Magnetic confinement of the solar tachocline*, Astronomy and Astrophysics, 457 (2006), pp. 665–674.

[3] J. Christensen-Dalsgaard et al., *The current state of solar modeling*, Science, 272 (1996), pp. 1286–1292.

[4] V. C. A. Ferraro, *The non-uniform rotation of the sun and its magnetic field*, Monthly Notices of the Royal Astronomical Society, 97 (1937), pp. 458–472.

[5] P. Garaud and L. A. Arreguin, *On the penetration of meridional circulation below the solar convection zone. ii. models with convection zone, the taylor-proudman constraint, and applications to other stars*, The Astrophysical Journal, 704 (2009), pp. 1–16.

[6] D. O. Gough and M. E. McIntyre, *Inevitability of a magnetic field in the sun's radiative interior*, Nature, 394 (1998), pp. 755–757.

[7] L. Mestel and N. O. Weiss, *Magnetic fields and non-uniform rotation in stellar radiative zones*, Monthly Notices of the Royal Astronomical Society, 226 (1987), pp. 123–135.

[8] M. S. Miesch, *Large-scale dynamics of the convection zone and tachocline*, Living Reviews in Solar Physics, 2 (2005).

[9] J. M. Pasachoff, V. Rusin, H. Druckmullerova, M. Saniga, M. Lu, C. Malamut, D. B. Seaton, L. Golub, A. J. Engell, S. W. Hill, and R. Lucas, *Structure and dynamics of the 2010 July 11 eclipse white-light corona*, The Astrophysical Journal, 734 (2011).

[10] J. Schou et al., *Helioseismic studies of differential rotation in the solar envelope by the solar oscillations investigation using the Michelson Doppler imager*, The Astrophysical Journal, 505 (1998), pp. 390–417.

[11] A. Skumanich, *Time scales for Ca II emission decay, rotational braking, and lithium depletion*, The Astrophysical Journal, 171 (1972), pp. 565–567.

[12] E. A. Spiegel and G. Veronis, *On the Boussinesq approximation for a compressible fluid*, The Astrophysical Journal, 131 (1960), pp. 442–447.

[13] E. A. Spiegel and J.-P. Zahn, *The solar tachocline*, Astronomy and Astrophysics, 265 (1992), pp. 106–114.

[14] A. Strugarek, A. S. Brun, and J.-P. Zahn, *Magnetic confinement of the solar tachocline: II. coupling to a conveciton zone*, Astronomy and Astrophysics, 532 (2011), p. A34.

[15] T. S. Wood, J. O. McCaslin, and P. Garaud, *The sun's meridional circulation and interior magnetic field*, The Astrophysical Journal, 738 (2011).